Electronic Supplementary Material (ESI) for Chemical Science.
This journal is © The Royal Society of Chemistry 2021

Supporting Information

Content

- Pictures of setup
- Comparison of sensing setups
- SEM images of samples
- IR spectroscopy data
- Additional uptake data
- LDA analysis
- Data for dew point experiments

Further uploaded files:

- Program code for Python
  - photoprogrammable electronic nose.ipynb
- Experimental data for kNN analysis for Figure 5
  - All-0%-cis-butanol.xlsx
  - All-0%-cis-cyclohexane.xlsx
  - All-0%-cis-n-hexane.xlsx
  - All-0%-cis-propanol.xlsx
  - All-86%-cis-butanol.xlsx
  - All-86%-cis-cyclohexane.xlsx
  - All-86%-cis-n-hexane.xlsx
  - All-86%-cis-propanol.xlsx
  - photoprogrammed-butanol.xlsx
  - photoprogrammed-cyclohexane.xlsx
  - photoprogrammed-n-hexane.xlsx
  - photoprogrammed-propanol.xlsx

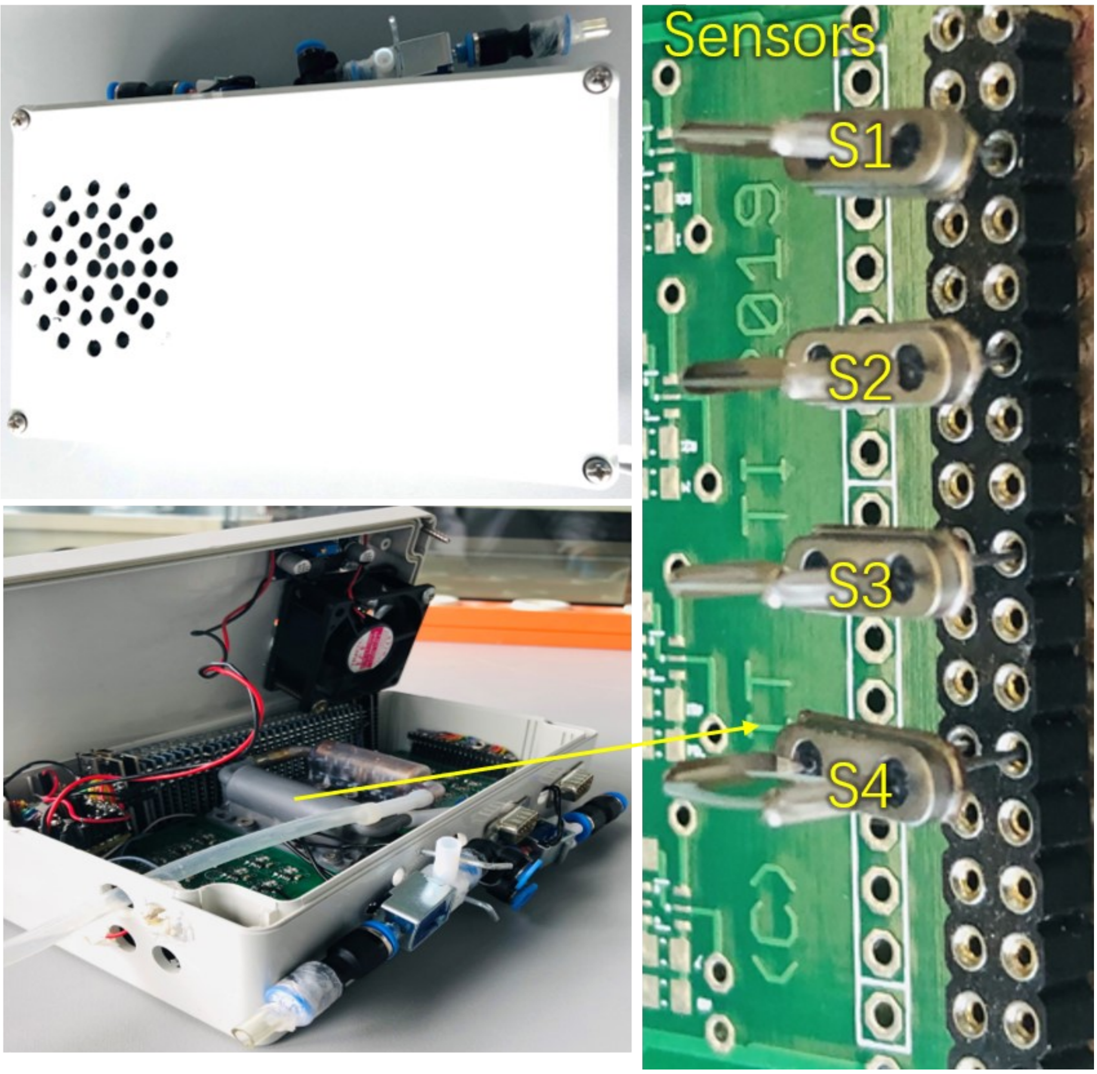

Figure SI1. Photographs of the setup and sensor array.

Table SI1: Comparison of different sensor techniques.

Sensor type	Operating Temp	Power consumption	Sensitivity	Selectivity	Reproducibility	Response time	Ref.
metal-oxide semi-conductor	~300-400°C	High	>0.1ppm	Poor	Moderate	Fast	[1-4]
Conducting polymer	Ambient	Low	0.01ppm	Moderate	Good	Moderate	[4-5]
Quartz crystal micro-balance	Ambient	Low	>0.1ppm	Poor to high[#]	Moderate[#]	Slow to fast[#]	[4, 6-7]
surface acoustic wave	Ambient	Low	ppb	Poor to high[#]	Moderate[#]	Slow to fast[#]	[4, 8-9]
gas chroma-tography	Ambient-elevated	Very high	ppt-ppq	High	Good	Slow / Very slow	[10-16]

Notes:

[#] Depending on the surface functionalization.

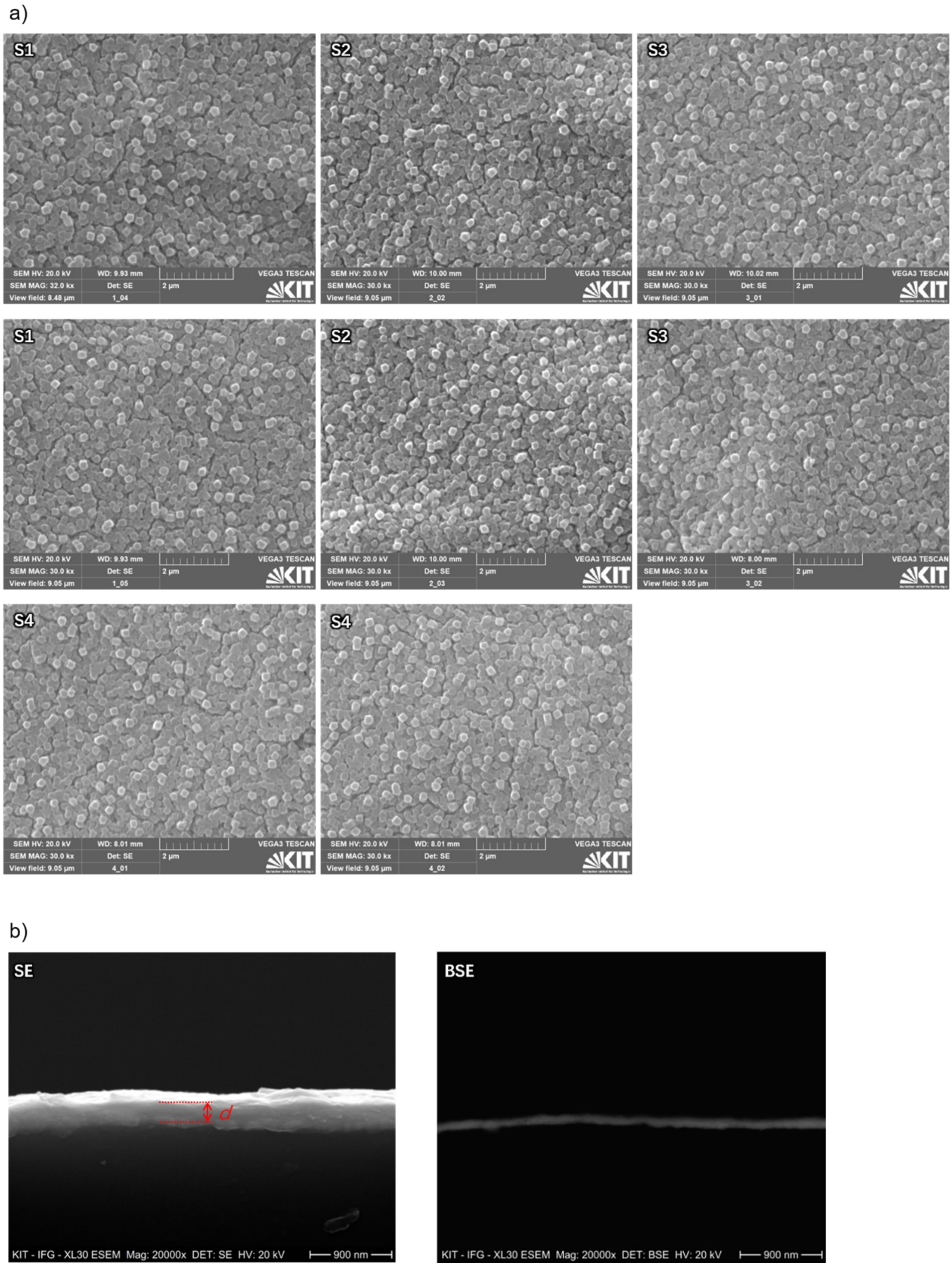

Figure SI2. Scanning electron microscopy (SEM) of the samples. The sample names (S1, S2, S3 and S4), the scale bares as well as the parameters are given in the images. a) Top view images of all 4 samples. All top view images are recorded with the secondary electron (SE) detector.

b) Cross-section of sample S2. The left image is taken with the SE detector. The right image is taken with the back-scattered electron (BSE) detector, showing the silver layer of the substrate. The thickness *d* of the SURMOF on the silver film is estimated to 0.2 µm.

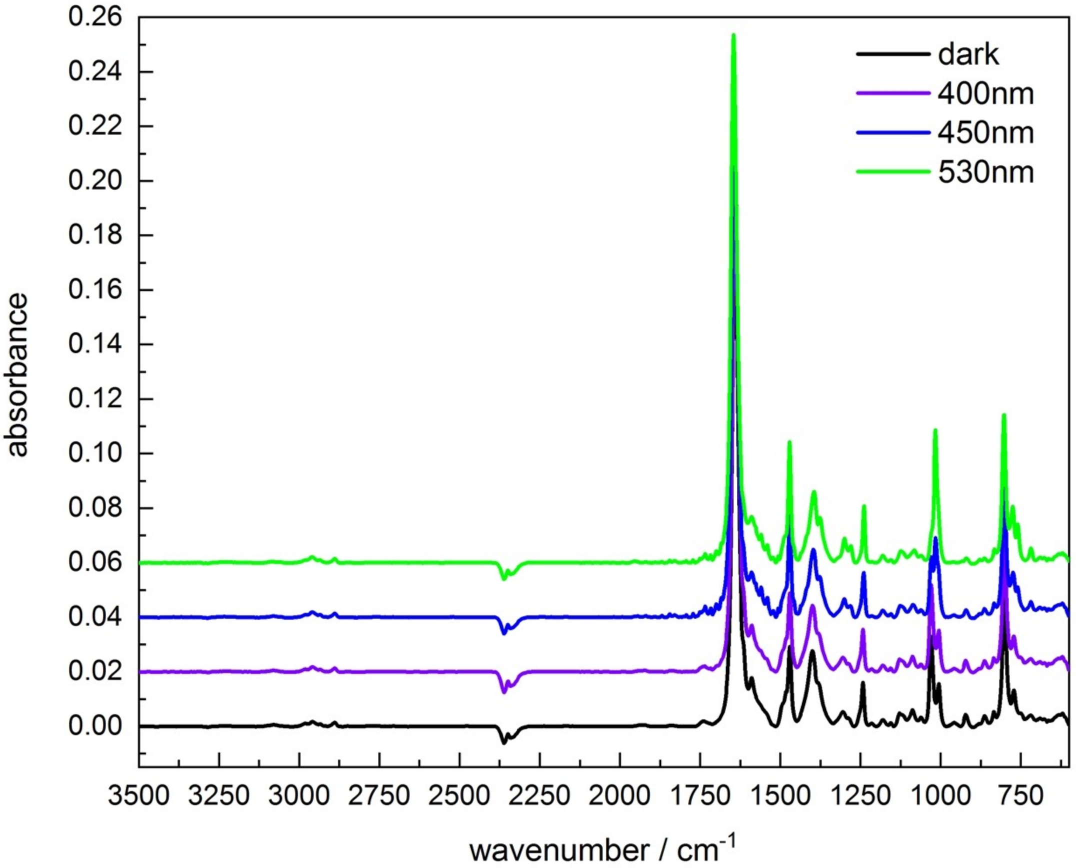

Figure SI3: IRRA spectra of the $Cu_2(F_2AzoBDC)_2(dabco)$ SURMOF. The thermally-relaxed sample (100% *trans*) is labeled as dark (black). The sample upon irradiation with violet, blue and green light are shown in violet, blue and green.

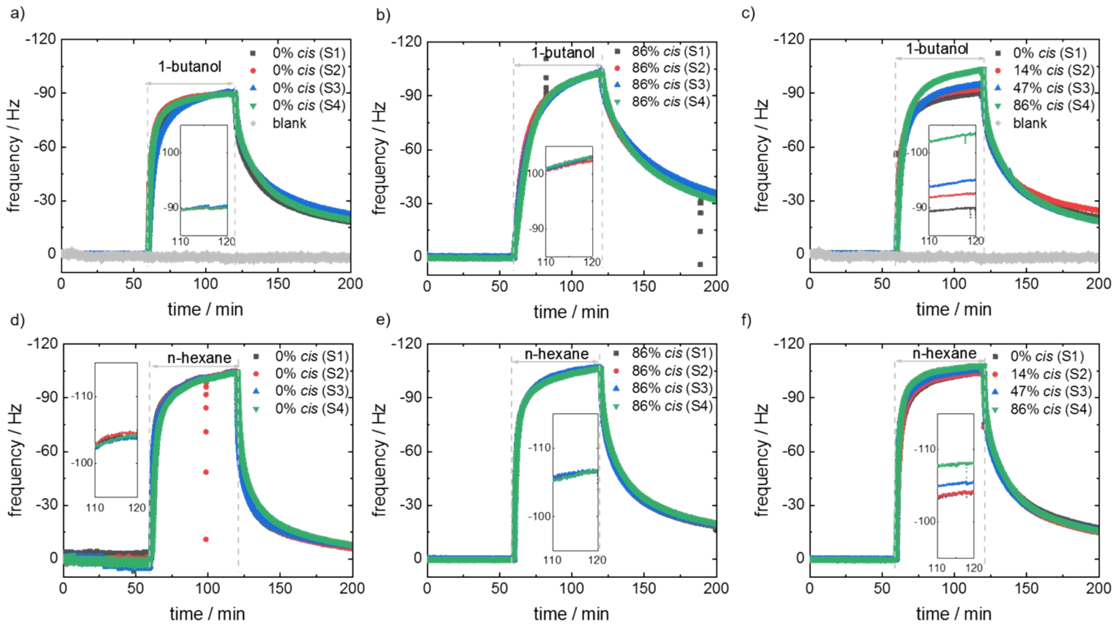

Figure SI4. E-nose responses to the exposure to 1-butanol (a-c) and n-hexane (d-f) vapor as a function of time. All azobenzene-groups in the sensor array are in the 100%-*trans* state in a) and d) and in the 86%-*cis*-state in b) and e). In panel c) and f), the sensor array is photoprogrammed so that the azobenzene groups are in 100%-*trans* (0%-*cis*) in sensor 1 (S1), 14%-*cis* in sensor 2 (S2), 47%-*cis* in sensor 3 (S3) and 86%-*cis* in sensor 4 (S4). The light-grey data in panel a) and c) are from the blank reference sample. The insets show zoom-ins of the data at the end of the analyte exposure where the y-scale is 20 Hz.

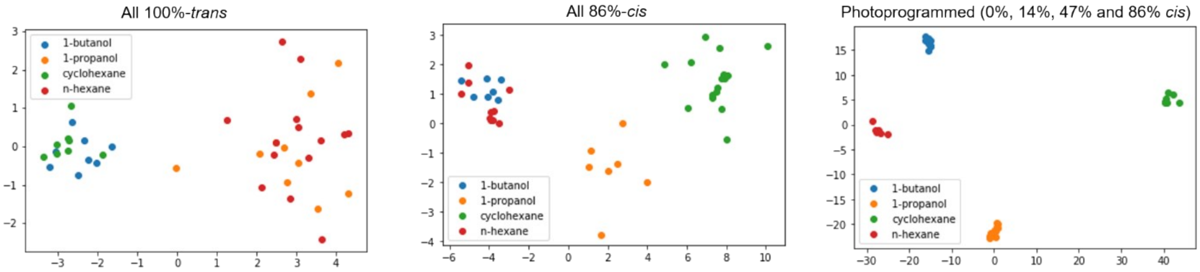

Figure SI5. Linear discriminant analysis (LDA) of the VOC data recorded with the e-nose where all sensors are in the 100%-*trans*-state (left), in the 86%-*cis*-state (center) and in the selectively photoprogrammed state (S1 0%, S2 14, S3 47% and S4 86% *cis*, right). The axes are the linear discriminants LD1 and LD2. The molecules are labelled in the legend. The discrimination accuracies are 47.1% (left), 81.5% (center) and 100% (right).

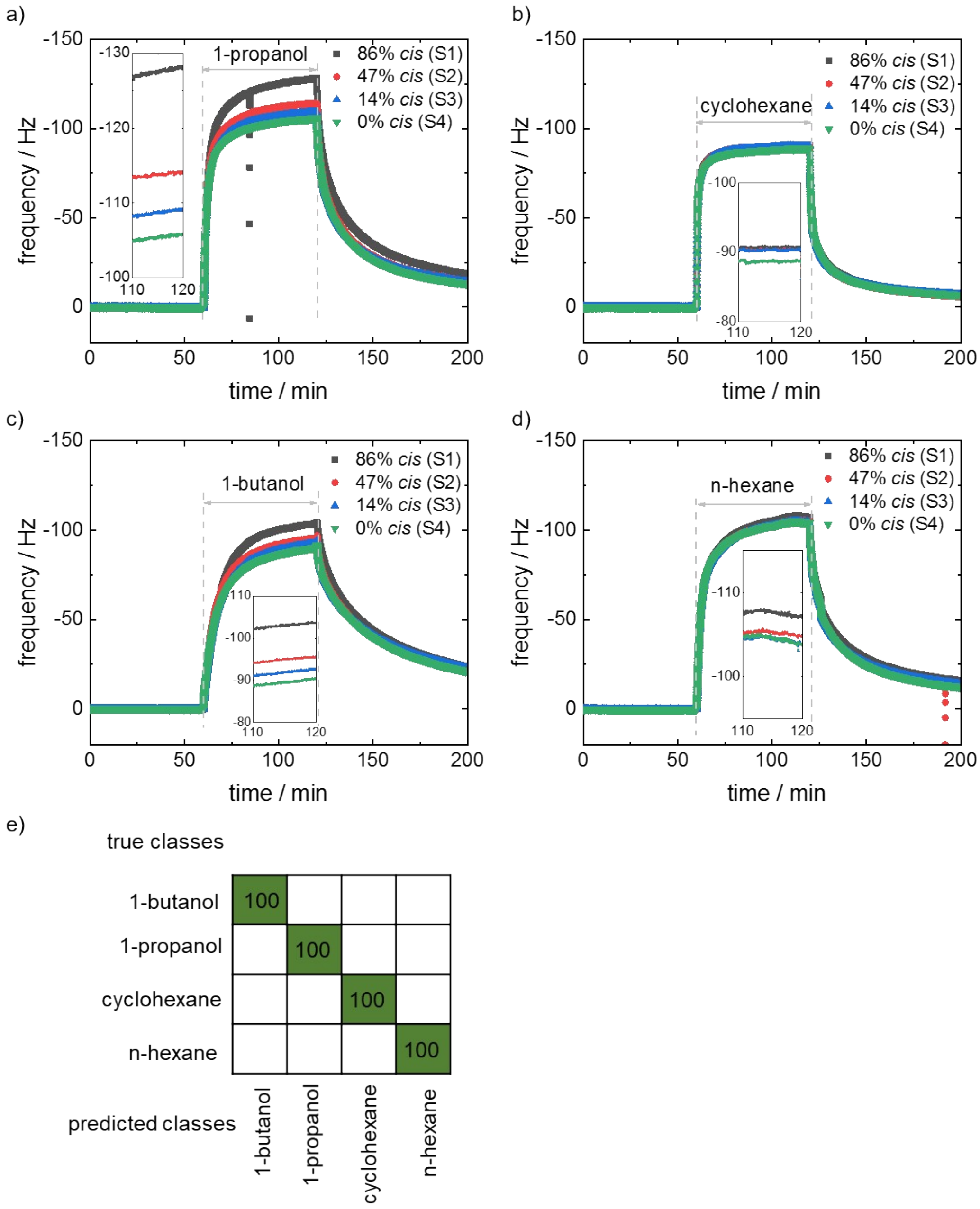

Figure SI6. E-nose response to the exposure to 1-propanol (a), cyclohexane (b), 1-butanol (c) and n-hexane (d) vapor as a function of time. The sensor array is photoprogrammed so that the azobenzene groups are in 86%-*cis* in sensor 1 (S1), 47%-*cis* in sensor 2 (S2), 14%-*cis* in sensor 3 (S3) and 0%-*cis* (100%-*trans*) in sensor 4 (S4). **e)** Confusion matrix of the 4 molecules and their classification. The insets show zoom-ins of the data at the end of the analyte exposure.

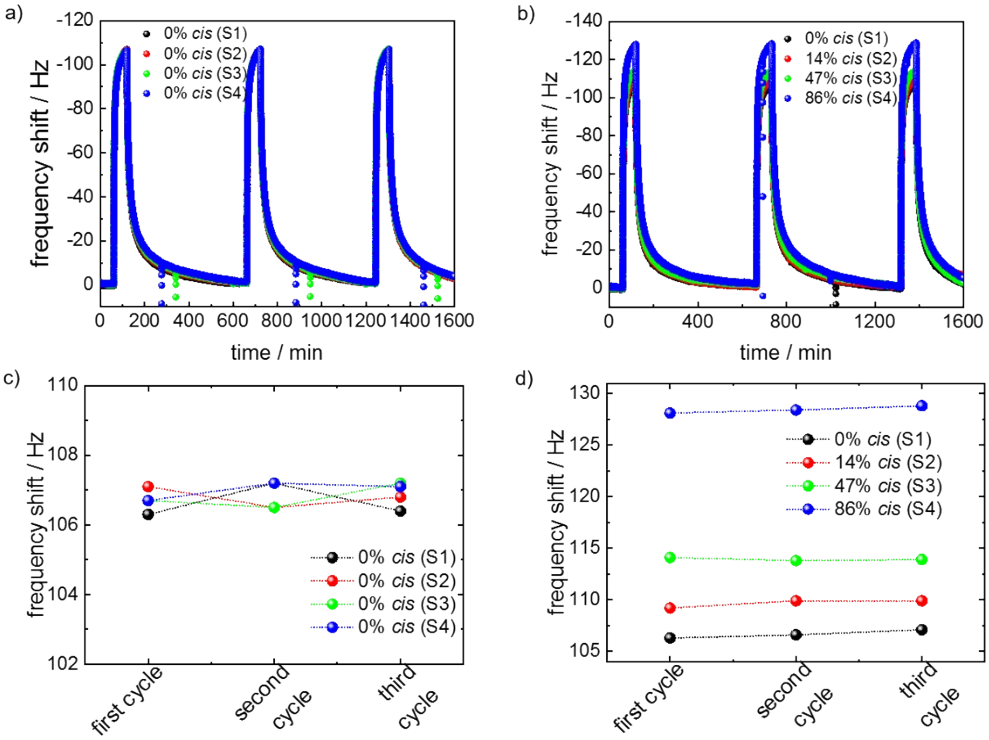

Figure SI7: E-nose response to the exposure to 1-propanol for 3 consecutive cycles. The sensors of the array are in the 100%-*trans* state in a) and c) and in the photoprogrammed-state in b) and d), i.e. 0%-*cis* in sensor 1 (S1), 14%-*cis* in sensor 2 (S2), 47%-*cis* in sensor 3 (S3) and 86%-*cis* in sensor 4 (S4). The time course of the sensor signal is shown in a) and b). The sensor signals at the end of the VOC exposure are shown in c) and d). The standard deviations of the three measurements of each individual sensor are between 0.26 Hz and 0.49 Hz in c) and 0.15 Hz and 0.4 Hz in d).

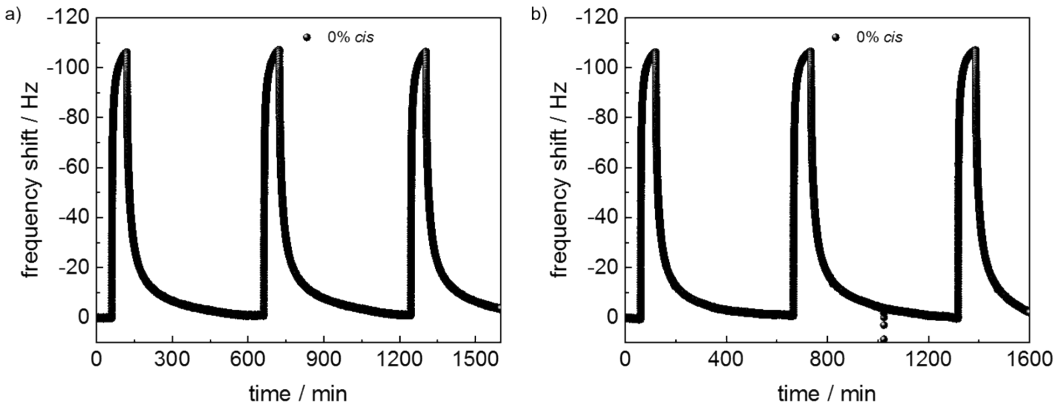

Figure SI8: E-nose response to the exposure to 1-propanol for 3 consecutive cycles. The sensor is in the 100%-*trans* state. The data in a) were recorded with the pristine sample, the data in b) were recorded after 1 week. The sample was stored in pure nitrogen. The standard deviation of the signal response at the end of the three VOC exposure cycles is 0.5 Hz in a) and 0.4 Hz in b). The difference between the mean values is approximately 0.1 Hz.

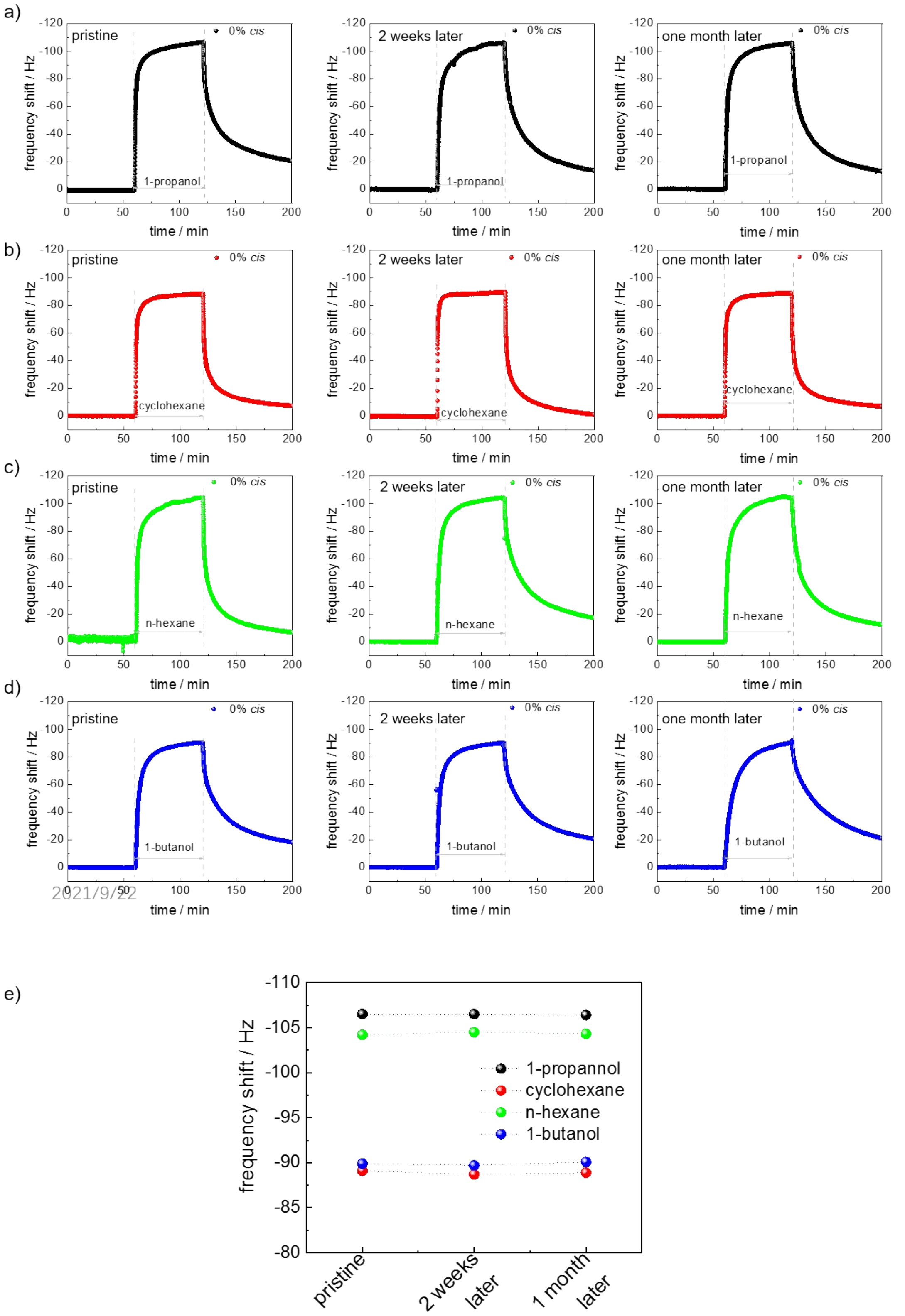

Figure SI9: E-nose response to the exposure to 1-propanol (a, black), cyclohexane (b, red), n-hexane (c, green) and 1-butanol (e, blue). The sensor is in the 100%-*trans* state. The data are recorded with the pristine sample (left-hand side), the data are recorded after 2 week (center) and after 1 month (right-hand side). The sample was stored in pure nitrogen. **e)** The comparison of the observed frequency shifts at the end of the VOC exposure (d) show signal changes of less than 0.4 Hz.

SI: Vapor pressure determination by dew point

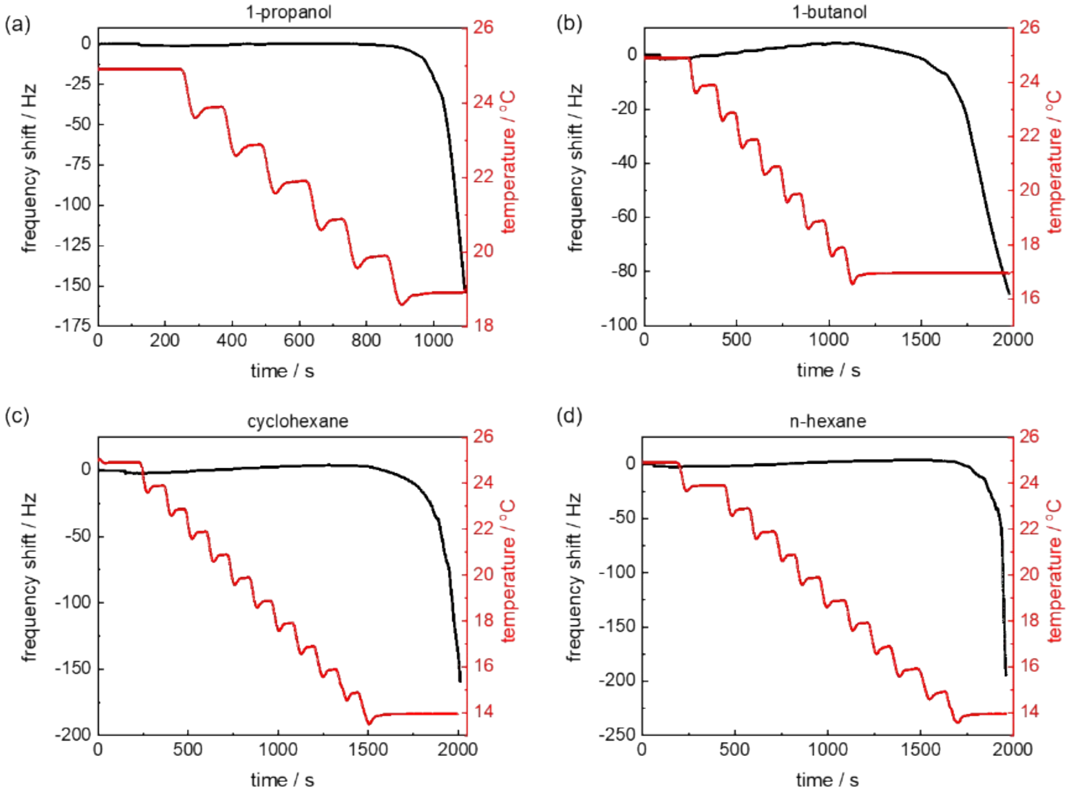

Figure SI10: Dew points of VOC vapors. The gas flows enriched with the vapors of 1-propanol (a), 1-butanol (b), cyclohexane (c) and n-hexane (d) were flowing over a blank QCM sensor. The temperature of the QCM sensor was decreased step-by-step, starting from 25°C with 1°C step size. The vapors were made by bubbling the nitrogen gas flow through the wash bottles at room temperature, 23°C, see experimental section and figure 1b. When the temperature of the QCM sensors was below the dew point of the vapor, the vapor condensed and the mass on the QCM sensor increased, i.e. the frequency shift decreased. The determined dew points are 19°C for 1-propanol, 17°C for 1-butanol, 14°C for cyclohexane and 14°C for n-hexane. This corresponds to vapor pressures of 19 mbar for 1-propanol, 5 mbar for 1-butanol, 78 mbar for cyclohexane and 124 mbar for n-hexane.

Table. Saturated vapor pressure of the targeted VOCs at 23 °C.

	Vapor Pressure / bar	**Ref.**
1-propanol	0.025	[17]
n-hexane	0.185	[18-19]
1-butanol	0.0078	[17]
cyclohexanone	0.119	[18, 20]

Table. Saturated vapor pressure of the targeted VOCs at the determined dew temperatures.

	dew temperature / °C	**Vapor Pressure / bar**	**Ref.**
1-propanol	19	0.0193	[17]
n-hexane	14	0.124	[18-19]
1-butanol	17	0.0052	[17]
cyclohexanone	14	0.078	[18, 20]

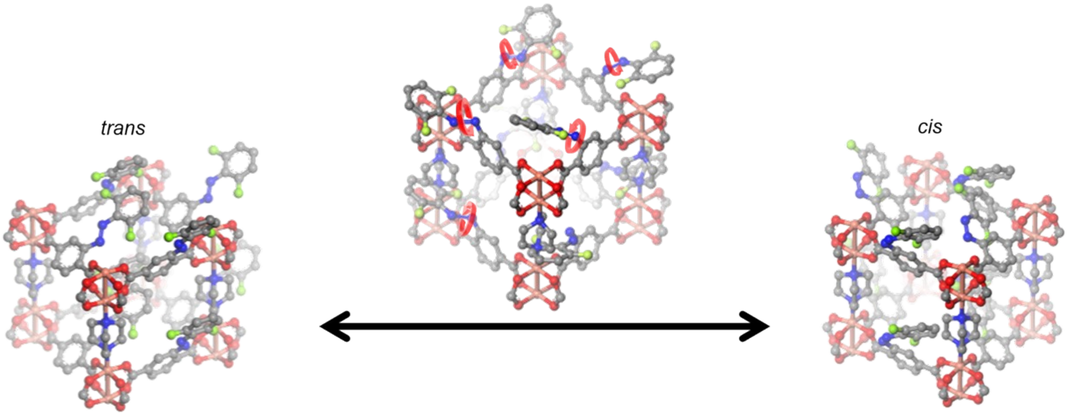

Figure SI11: The structure of $Cu_2(F_2AzoBDC)_2$(dabco). The azobenzene side groups of the SURMOF can isomerize from the *trans* form (left-hand side) to the *cis* form (right-hand side) and *vice versa*. Since the isomerization occurs upon excitation of the n-π* transition with visible light, the *trans-cis* isomerization process of the azobenzene moiety most likely happens via rotation around the N=N bond.[21-22] The transition state with red arrows indicating the rotation is sketched in the center. There is sufficient space in the MOF pores for the *trans-cis* isomerization. Carbon atoms are shown in gray, oxygen in red, copper in orange, fluorine in green and nitrogen in blue. Hydrogen atoms have been omitted.

References:

1. I.Lundström; A.Spetz; F.Winquist; U.Ackelid; H.Sundgren, Catalytic metals and field-effect devices—a useful combination. *Sensors and Actuators B: Chemical* **1990,** *1* (1-6), 15-20.
2. W.Gardner, J.; V.Shurmer, H.; PaulCorcoran, Integrated tin oxide odour sensors. *Sensors and Actuators B: Chemical* **1991,** *4* (1-2), 117-121.
3. W.Gardner, J.; N.Bartlett, P., A brief history of electronic noses. *Sensors and Actuators B: Chemical* **1994,** *18* (1-3), 210-211.
4. Karakaya, D.; Ulucan, O.; Turkan, M., Electronic Nose and Its Applications: A Survey. *International Journal of Automation and Computing* **2019,** *17* (2), 179-209.
5. N.Bartlett, P.; B.M.Archer, P.; K.Ling-Chung, S., Conducting polymer gas sensors part I: fabrication and characterization. *Sensors and Actuators* **1989,** *19* (2), 125-140.
6. Thies, J. W.; Kuhn, P.; Thürmann, B.; Dübel, S.; Dietzel, A., Microfluidic quartz-crystal-microbalance (QCM) sensors with specialized immunoassays for extended measurement range and improved reusability. *Microelectronic Engineering* **2017,** *179*, 25-30.
7. M.Haug; K.D.Schierbaum; G.Gauglitz; W.Göpel, Chemical sensors based upon polysiloxanes: comparison between optical, quartz microbalance, calorimetric, and capacitance sensors. *Sensors and Actuators B: Chemical* **1993,** *11* (1-3), 383-391.
8. Shaffer, R. E.; Rose-Pehrsson, S. L.; McGill, R. A., Multiway Analysis of Preconcentrator-Sampled Surface
Acoustic Wave Chemical Sensor Array Data. *Field Analytical Chemistry & Technology* **1998,** *2* (3), 179-192.
9. Liron, Z.; Kaushansky, N.; Frishman, G.; Kaplan, D.; Greenblatt, J., The polymer-coated SAW sensor as a gravimetric sensor. *Analytical Chemistry* **1997,** *69* (14), 2848-2854.
10. Wunsch, M. R.; Reiter, A. M. C.; Schuster, F. S.; Lehnig, R.; Trapp, O., Continuous online process analytics with multiplexing gas chromatography by using calibrated convolution matrices. *J Chromatogr A* **2019,** *1595*, 180-189.
11. Anderson, J. L.; Armstrong, D. W., Immobilized Ionic Liquids as High-Selectivity/
High-Temperature/High-Stability Gas
Chromatography Stationary Phases. *Anal. Chem.* **2005,** *77*, 6453-6462.
12. J.Buijten; L.Blomberg; S.Hoffmann; K.Markides; T.Wännmann, Use of poly(silarylene-methylphenylsiloxane) block copolymer as a thermostable stationary phase in capillary column gas chromatography. *Journal of Chromatography A* **1984,** *301*, 265-269.
13. Poole, C. F.; Poole, S. K., Ionic liquid stationary phases for gas chromatography. *J Sep Sci* **2011,** *34* (8), 888-900.
14. Allwood, J. W.; Erban, A.; de Koning, S.; Dunn, W. B.; Luedemann, A.; Lommen, A.; Kay, L.; Loscher, R.; Kopka, J.; Goodacre, R., Inter-laboratory reproducibility of fast gas chromatography-electron impact-time of flight mass spectrometry (GC-EI-TOF/MS) based plant metabolomics. *Metabolomics* **2009,** *5* (4), 479-496.
15. Syhre, M.; Chambers, S. T., The scent of Mycobacterium tuberculosis. *Tuberculosis (Edinb)* **2008,** *88* (4), 317-23.
16. Denawaka, C. J.; Fowlis, I. A.; Dean, J. R., Evaluation and application of static headspace-multicapillary column-gas chromatography-ion mobility spectrometry for complex sample analysis. *J*

Chromatogr A **2014,** *1338*, 136-48.

17. Kemme, H. R.; Kreps, S. I. J. J. o. C.; Data, E., Vapor pressure of primary n-alkyl chlorides and alcohols. **1969,** *14* (1), 98-102.

18. Li, I. P.; Lu, B. C.; Chen, E. J. J. o. C.; Data, E., Vapor-Liquid equilibriums of binary systems containing n-hexane, cyclohexane, and benzene at low temperatures. **1973,** *18* (3), 305-309.

19. Rossini, D., VAPOR PRESSURES AND BOILING POINTS OF SOME PARAFFIN, ALKYLCYCLOPENTANE, ALKYLCYCLOHEX" ANE, AND ALKYLBENZENE~ HYDROCARBONSI. **1945**.

20. Gaw, W.; Swinton, F. J. T. o. t. F. S., Thermodynamic properties of binary systems containing hexafluorobenzene. Part 3.—Excess Gibbs free energy of the system hexafluorobenzene+ cyclohexane. **1968,** *64*, 637-647.

21. Bandara, H. M. D.; Burdette, S. C., Photoisomerization in different classes of azobenzene. *Chem. Soc. Rev.* **2012,** *41* (5), 1809-1825.

22. Knie, C.; Utecht, M.; Zhao, F. L.; Kulla, H.; Kovalenko, S.; Brouwer, A. M.; Saalfrank, P.; Hecht, S.; Bleger, D., ortho-Fluoroazobenzenes: Visible Light Switches with Very Long-Lived Z Isomers. *Chemistry-a European Journal* **2014,** *20* (50), 16492-16501.